Supplementary Information

A Magnetic Responsive Composite Surface for High-Performance Droplet and Bubble Manipulation

Cong Liu [ab], Jinxia Huang [b*] ,Zhiguang Guo [ab*] and Weimin Liu [b]

[a] Ministry of Education Key Laboratory for the Green Preparation and Application of Functional Materials, Hubei University, Wuhan 430062, People's Republic of China

[b] State Key Laboratory of Solid Lubrication, Lanzhou Institute of Chemical Physics, Chinese Academy of Sciences, Lanzhou 730000, People's Republic of China

E-mail: zguo@licp.cas.cn and huangjx@licp.cas.cn ; Fax: +86-931-8277088; Tel.: +86-931-4968105

Supplementary Information contains:

Supplementary Methods

Magnetically Controlled Sliding Mechanism

Supplementary Fig. S1−S13

Movie S1-S4

References

Supplementary methods:

Materials

Cobalt microparticles (MPs, average diameter of 1-5 μm) was purchased from Beijing Yannuo Xincheng Technology Co., Ltd. Poly-dimethylsiloxane (PDMS) silicone elastomer (Sylgard 184A) and curing agent (Sylgard 184B) were obtained from the Dow chemical Co., Ltd. Dimethyl silicone oil (viscosity of 10 cSt at 25℃) was obtained from Shanghai Aladdin Biochemical Co., Ltd. Formamide was bought from Shanghai Aladdin Biochemical Co., Ltd. A zinc plate (99%, 20 × 20 × 10 mm) was obtained from Hefei Wenghou Co., Ltd. All of other chemical reagents were of analytical grade and used without further purification. Deionized water was produced using a Modupure system and was used in all experiments.

Sample preparation

Preparation of ZnO nanoarray According to previous literatures, we fabricated ZnO nanoarrays on Zn metal substrates using the natural oxidation of zinc metal in formamide/water mixtures.[1, 2] First, the zinc plates were ultrasonically cleaned in acetone and deionized water, respectively. Then the dried zinc plates were immersed in formamide solutions with different volume fractions (2%, 5%, 10%, 15%) for 24h at 65℃. Third, the plates were taken out of the solution and rinsed with alcohol and deionized water, and dried at room temperature for further experiments.

Preparation of Magnetic Responsive Composite Surface The PDMS elastomer precursor and curing agent (weight ratio 10 : 1) were fully stirred to obtain a homogeneous solution. Then, the cobalt MPs in different weight ratios was added into the same mass of PDMS in different weight ratios. After that, the above mixture was poured onto the ZnO nanoarray, and then placed in a vacuum chamber at -60 KPa to evacuate the air bubbles, followed by curing at 80 ℃ for 2 h. The Co/PDMS film was soaked in silicone oil for 30 min. Then the surface was vertically placed for 10 min to remove the excess silicone oil, and the magnetic responsive composite surface was obtained.

Characterization

The surface morphologies of samples were observed by a field emission scanning electron microscope (FESEM, JEOL JSM-6701F) with Au-sputtered samples. The crystal structure of as-prepared samples was characterized by means of X-ray diffraction (XRD) patterns (XRD, X'SPERT PRO). The values of contact angle and sliding angle were recorded by a JC10001 contact angle measure system (Zhongchen digital equipment Co., Ltd. Shanghai, China). The surface profile and roughness were characterized by 3D non-contact surface profiler (KLA-Tencor MicroXAM-800).

Magnetically Controlled Sliding Mechanism

In order to understand the regulation mechanism of the magnetic field during the movement of the droplet/bubble, we performed a force analysis on the sliding process of the droplet/bubble on the MRCS. As shown in Fig. S10, droplets deposited on the slippery composite surface were subjected to gravitation force (mg) and positive direction force (N). The driving force is the component of gravity when the droplet slides along the surface, which can be calculated as $F_{diving} = mg\sin\alpha$, where m is the mass of the droplet, α is the inclined angle of the slippery composite surface, and g is the gravitational acceleration. The resistance force was the surface retention force (F_r) and depends on the TCL and the CAH. When $F_{diving} > F_r$, the droplet began to slide on the MRCS. The contact angle hysteresis of a droplet can be calculated as $F_{CAH} = \Upsilon(\cos\theta_r - \cos\theta_a)$, where Υ is the surface tension of water and θ_r and θ_a represent the receding angle and advancing angle.[3,4] The length of the TCL (L_c) also greatly affects the sliding of the droplet on the smooth surface. When there is no magnetic field, a short three-phase contact line leads to a smaller CAH, as shown in the inset of Fig. S10a. When a magnetic field was applied to the slippery composite surface, rough cone-shaped structures were formed. In this case, the droplet is "clutched" by the magnetic cone, leading to a long TCL with a linear shape. The slip resistance of the droplet is proportional to the length L_c of the TCL.[5-7] Therefore, the resistance of

droplets in the presence of magnetic field is much larger than that in the absence of magnetic field. In addition, the existence of magnetic cone further leads to larger CAH. Therefore, the inclination angle of the slippery composite surface should be increase to overcome F_r and make the droplets slide. When the magnetic field was removed, the magnetic cone disappeared, the topography of the smooth composite surface returned to its initial state, and the droplets continued to slide.

Similarly, force analysis was performed on the sliding process of bubbles on the MRCS (Fig. S10b). The driven force of bubble motion is the axis-direction component of buoyancy (F_b), which can be computed as $F_{diving} = \rho g v \sin\beta$ (ρ, g, v, and β denote the water density, gravitational acceleration, bubble volume, and tilt angle of the slippery composite surface, respectively.) The adhesion force (F_a) of the slippery surface ensures that the bubbles interact with the composite surface in equilibrium with the buoyancy component perpendicular to the axial direction. Compared with the droplets in the air, the resistance of the bubbles in the aqueous environment during the sliding process includes the fluid drag (F_{drag}) caused by the impedance of the water in addition to the F_r and CAH generated by the TCL. In a viscous fluid, the fluid drag can be briefly expressed as $F_{drag} = 1/2\, C_D \rho v^2 S$, where S, v, and C_D, are the cross-sectional area of the bubble, the sliding velocity of the bubble, and the drag coefficient of water, respectively.[8,9] As shown in Fig. S10b, in the absence of a magnetic field, the bubbles only need to overcome a small resistance to slide on the MRCS. When a magnetic field was applied, the formation of magnetic cones increases the TCL of the bubbles and induces a larger CAH. At the initial lower inclination angle, it was not enough to support the sliding of the bubbles, resulting in in situ pinning of the bubbles on the MRCS (Fig. S10b). After removing the magnetic field, the magnetic cone disappears and the SA of the bubble returns to the initial state, which can continue to slide on the MRCS. By analyzing the driving mechanism of the MRCS, it is found that the magnetically responsive surface can reversibly manipulate droplets and bubbles in a non-contact manner with instantaneous response without polluting droplets/bubbles. This amphibious magnetic response surface has great application prospects in

microfluids and microchemical reactors.

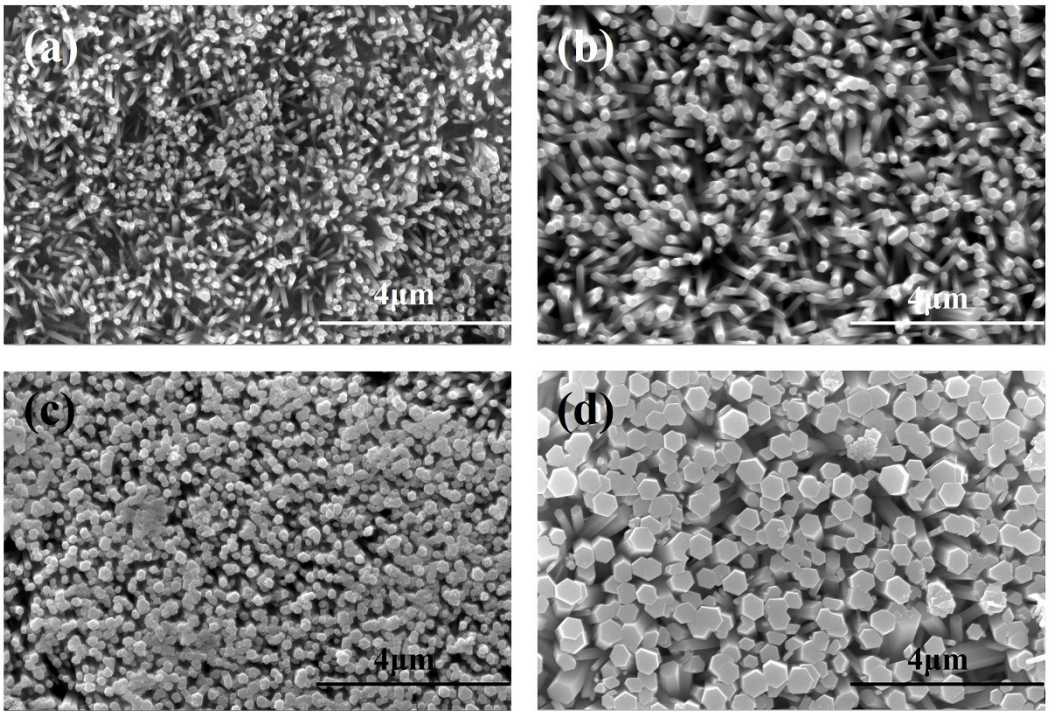

Fig. S1. SEM images of ZnO nanorod arrays grown on zinc foil with 24 h from (a) 2, (b) 5, (c) 10, and (d) 15 % formamide/water mixtures. With the increase of formamide content, the average nanorod diameter increased from 81.12, to 88.07, to 106.10, to 233.17 nm, respectively. The growth density of nanorods also gradually increased.

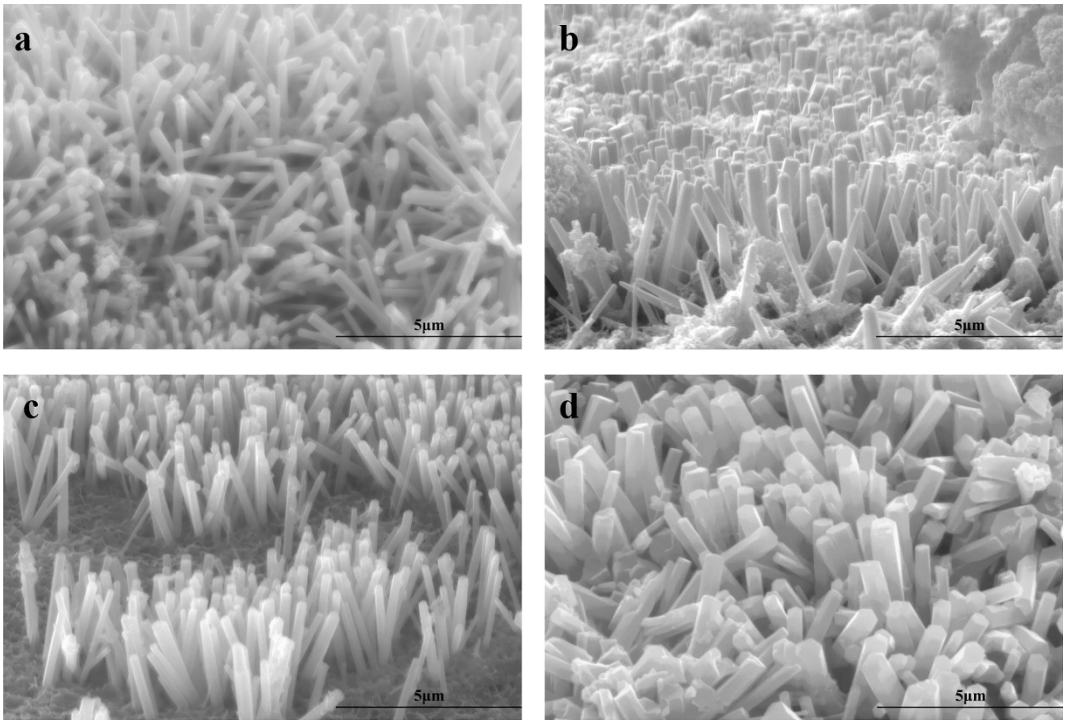

Fig. S2. SEM images of ZnO nanorod array heights after 24 h growth in mixtures of (a) 2, (b) 5, (c) 10 and (d) 15% formamide/water. With the increase of formamide content, the average height of the nanorods did not change significantly and remained in the range of 2.5–3 µm.

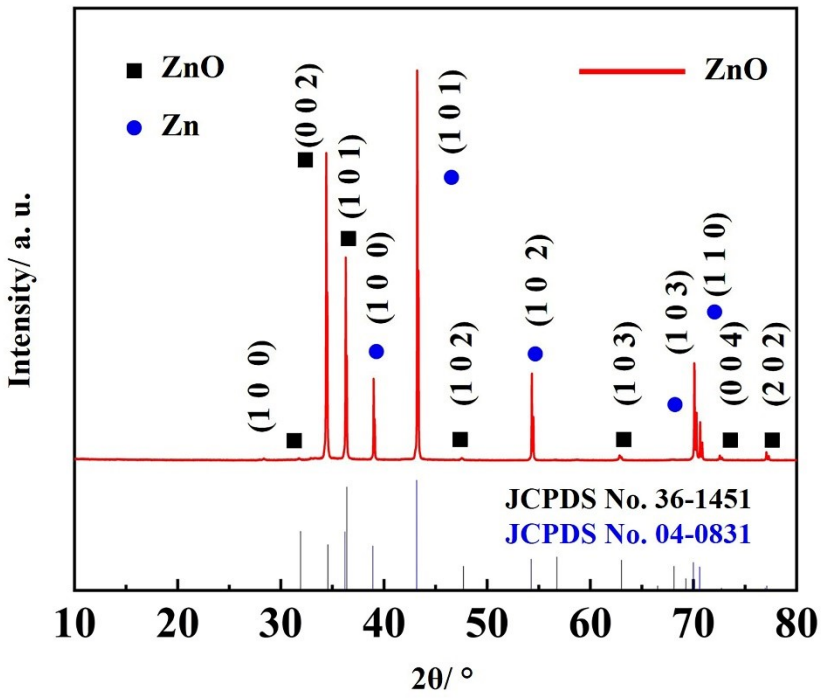

Fig. S3. XRD pattern of the as-prepared ZnO surface on the zinc substrate immersed in a 5% formamide/water mixture.

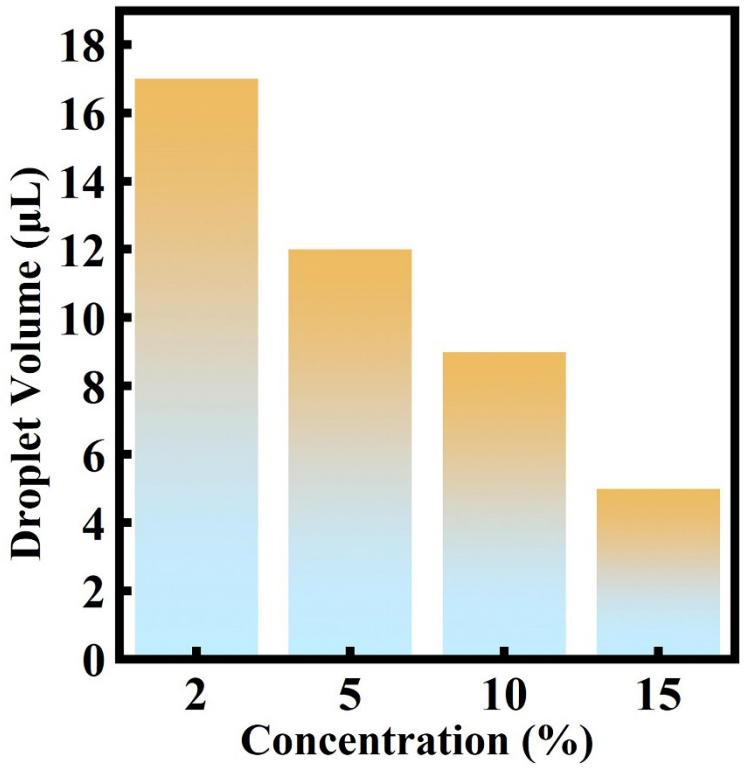

Fig. S4. Effect of formamide solution concentration on droplet transport.

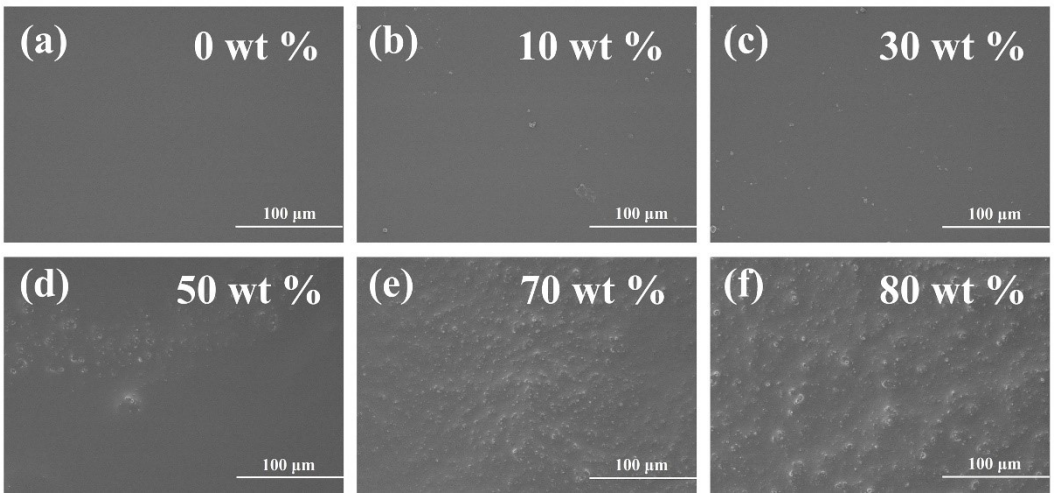

Fig. S5. SEM images of the Co/PDMS films containing (a) 0 wt % Co, (b) 10 wt % Co, (c) 30 wt % Co,(d) 50 wt % Co, (e) 70 wt % Co, (f) 80 wt % Co. With increasing cobalt content, the surface protrusions of the films increased.

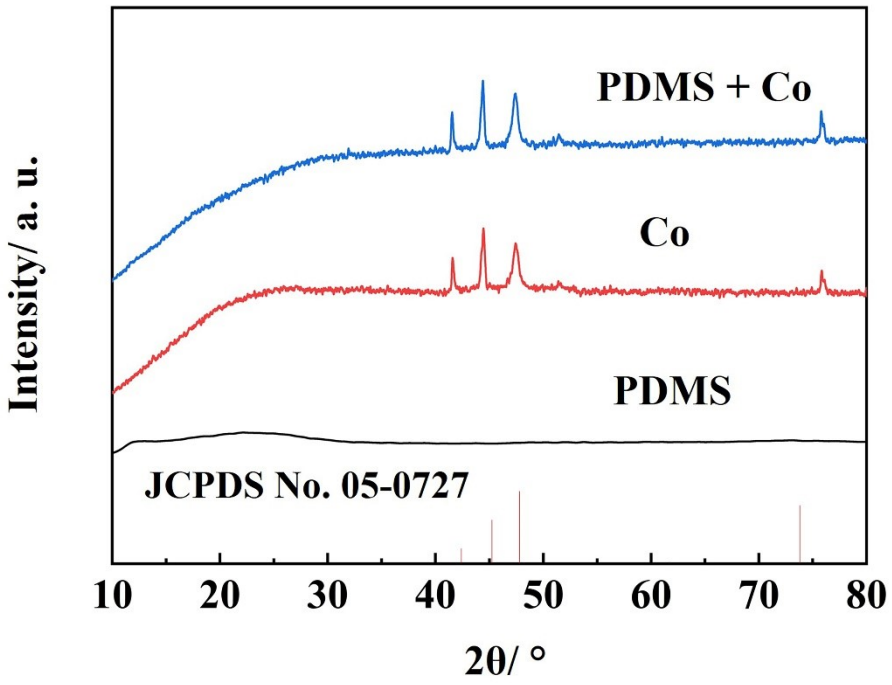

Fig. S6. XRD patterns of the Co, pristine PDMS, and Co_{70}/PDMS composite compared with the standard patterns for Co.

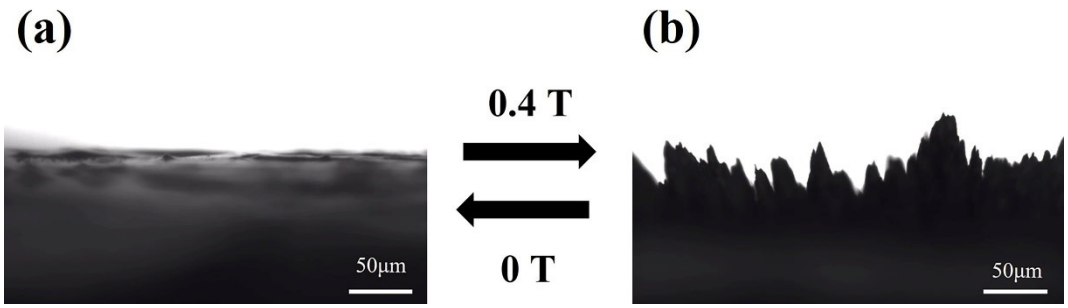

Fig. S7. The reversible formation of magnetic cone under 0 and 0.4 T magnetic fields. When an external magnetic field is applied perpendicular to the interface, the magnetic fluid self-assembles in rough magnetic cones modes that run along the direction of the magnetic vector lines. When the magnetic field is withdrawn, the cone disappeared to form a smooth interface again.

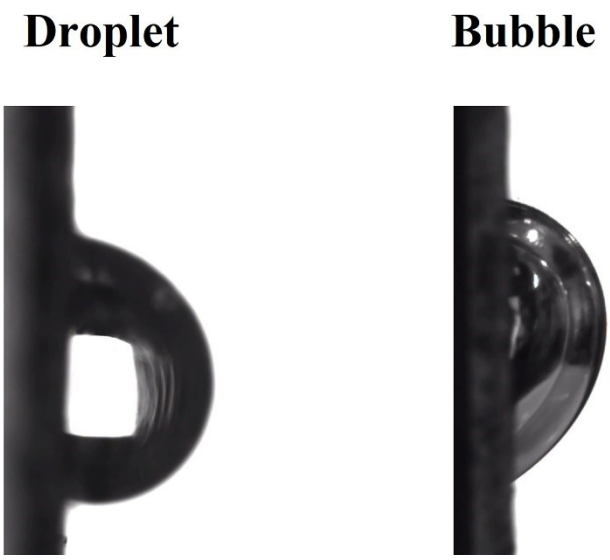

Fig. S8. Due to the large contact angle hysteresis of the pristine composite surface, a droplet and bubble cannot slide on the surface even if the surface was tilted at 90°.

Fig. S9. The CA of silicone oil the pristine composite film was approximately 0°, demonstrating silicone oil can be easily absorbed into the surface to form the slippery composite surface.

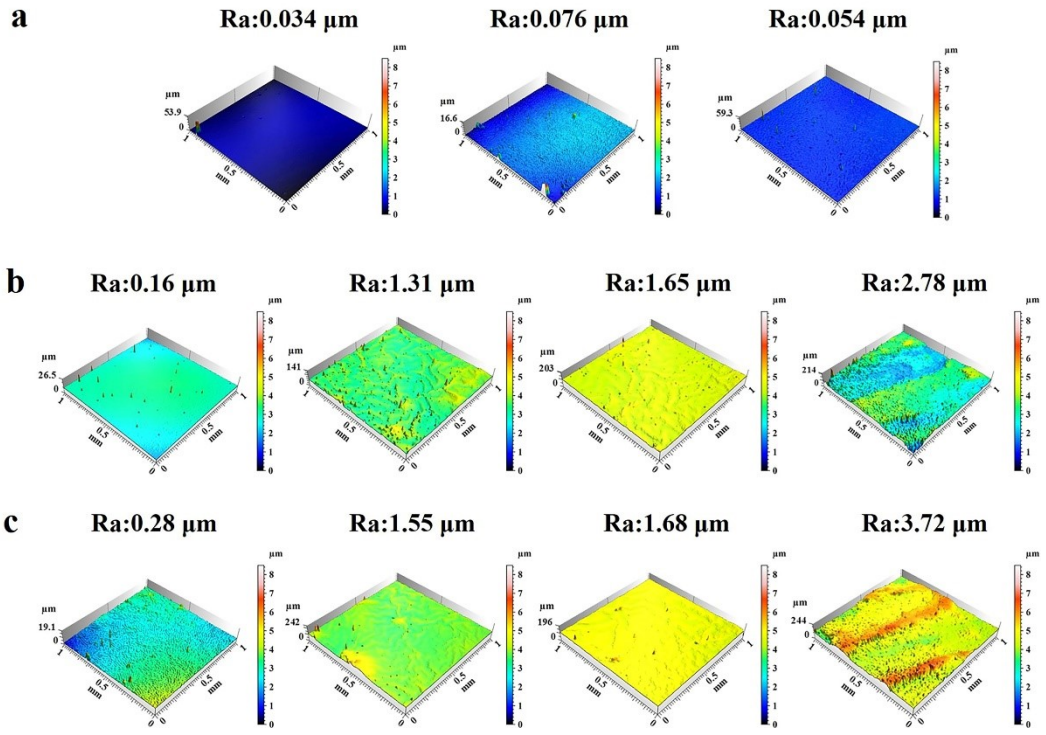

Fig. S10. (a) The 3D noncontact surface profiler images of 0 wt% under 0 T, 0.4 T and after removing the 0.4 T magnetic fields. (b) The 3D noncontact surface profiler images of the slippery Co_{10}/PDMS, Co_{30}/PDMS, Co_{50}/PDMS, Co_{80}/PDMS without applied magnetic field (Initial state). (c) The 3D noncontact surface profiler images of the slippery Co_{10}/PDMS, Co_{30}/PDMS, Co_{50}/PDMS, Co_{80}/PDMS after removing the 0.4 T magnetic fields. (Third state).

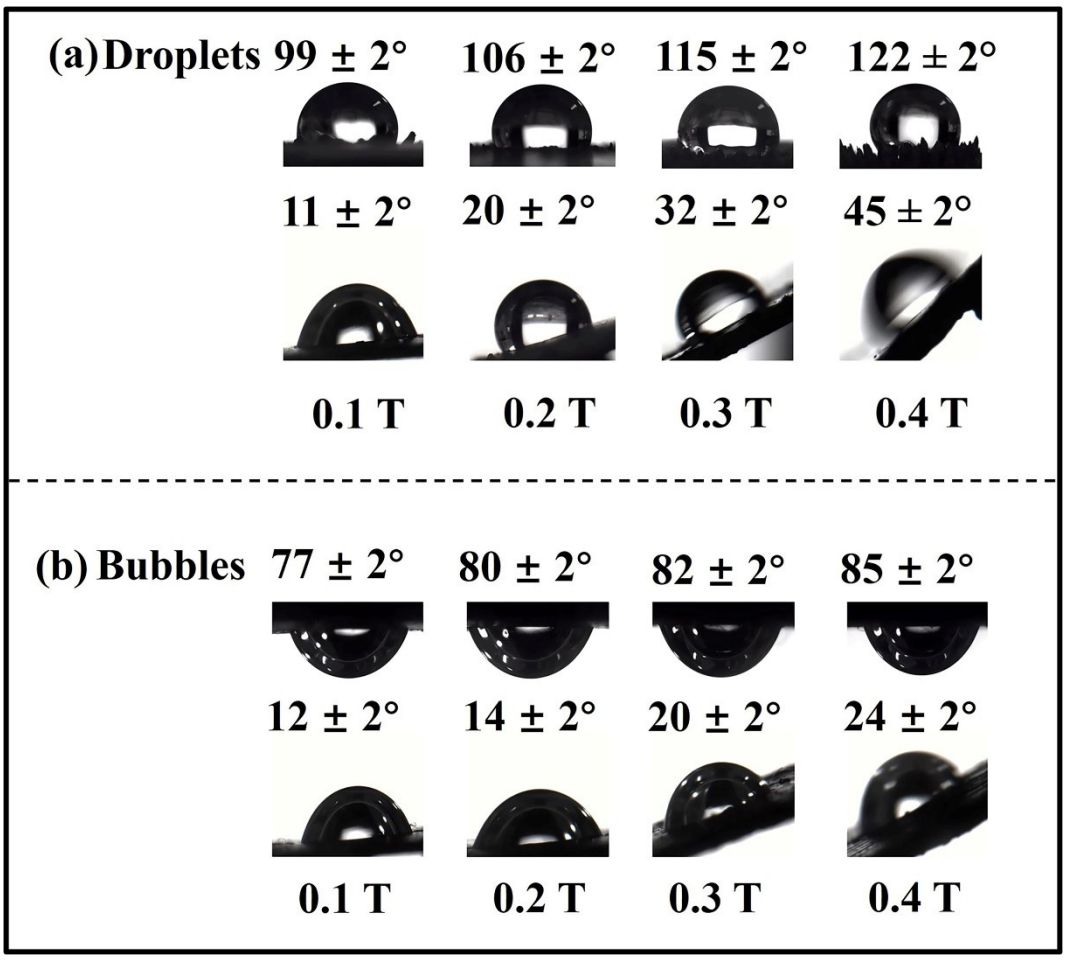

Fig. S11. Optical photographs of CAs and SAs of 5 μL (a) water droplets and (b) bubbles underwater on the slippery composite surfaces under different magnetic fields.

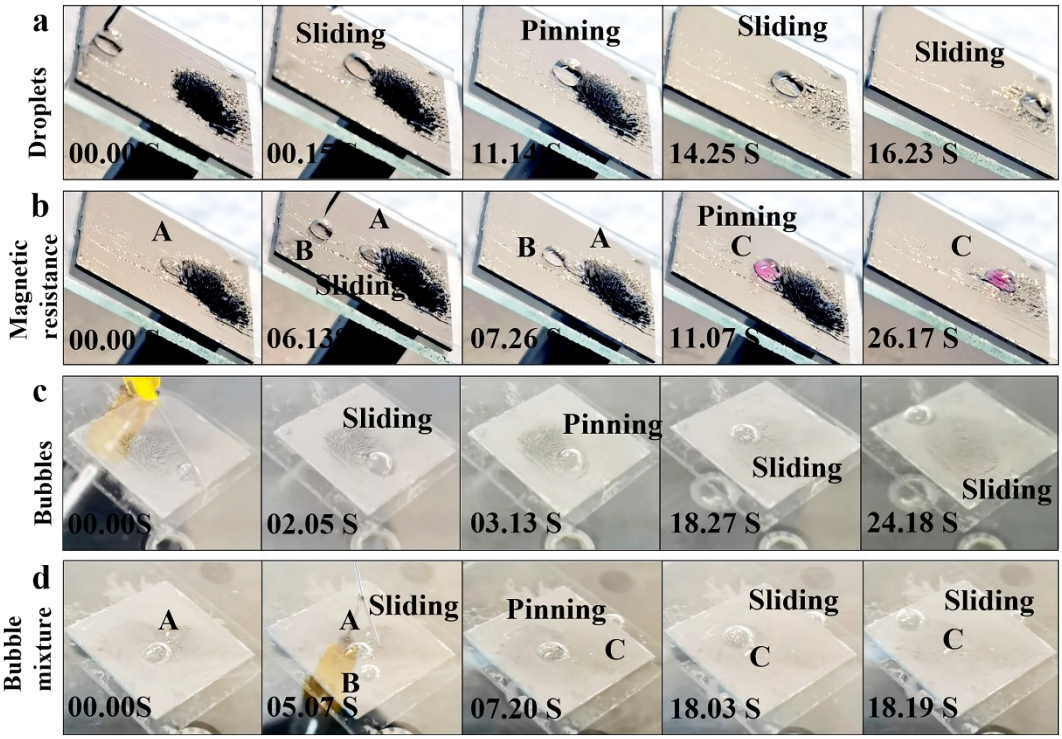

Fig. S12. (a) Demonstration of magnetically controlled droplet movement on MRCS. (b) Demonstration of magnetically controlled water droplet transport for a chemical reaction. (c) Demonstration of magnetically controlled bubble movement on the slippery composite surface. (d) Demonstration of magnetically controlled bubble mixture on the slippery composite surface.

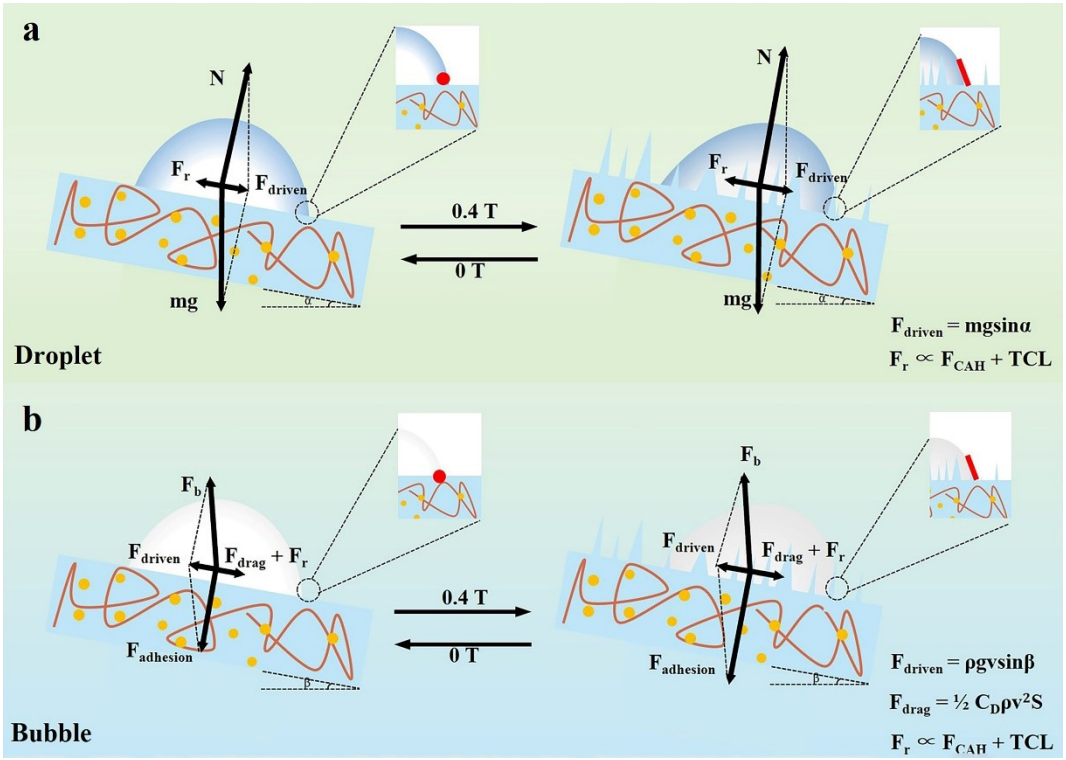

Fig. S13. Schematic diagram of force analysis of (a) droplet and (b) bubbles on a slippery composite surface. The inset is a schematic diagram of the corresponding three-phase contact line changes (red dots and lines).

References

1 X. Feng, L. Feng, M. Jin, J. Zhai, L. Jiang and D. Zhu, *J. Am. Chem. Soc.,* 2004, **126**, 62-63.

2 X. Jing and Z. Guo, *Nanoscale,* 2019, **11**, 8870-8881.

3 X. Yao, Y. Hu, A. Grinthal, T. S. Wong, L. Mahadevan and J. Aizenberg, *Nat Mater*, 2013, **12**, 529-534.

4 S. M. Kim, D. H. Kang, J. H. Koh, H. S. Suh, H. Yoon, K.-Y. Suh and K. Char, *Soft Mater*, 2013, **9**.

5 M. Cao, X. Jin, Y. Peng, C. Yu, K. Li, K. Liu and L. Jiang, *Adv. Mater.*, 2017, **29**,1606869

6 S. K. Alen, N. Farhat and M. A. Rahman, *AIP Conf. Proc*, 2016, 040030-1-040030-6.

7 J. Loudet, P. Hanusse and P. Poulin, *Scienc,.* 2004, **306**, 1525-1525.

8 J. Masliyah, R. Jauhari and M. Gray, *Chem. Eng. Sci.,* 1994, **49**, 1905-1911.

9 C. Zhang, B. Zhang, H. Ma, Z. Li, X. Xiao, Y. Zhang, X. Cui, C. Yu, M. Cao and L. Jiang, *ACS Nano*, 2018, **12**, 2048-2055.